The influence of intense control laser pulses on homodyne-detected rotational wave packet dynamics in O_2 by degenerate four-wave mixing

Vasilios G. Stavros, Elad Harel, and Stephen R. Leone
Department of Chemistry and Department of Physics, University of California, Berkeley, California 94720 and Lawrence Berkeley National Laboratories, University of California, Berkeley, California 94720

(Received 20 October 2004; accepted 12 November 2004; published online 24 January 2005)

We illustrate how the preparation and probing of rotational Raman wave packets in O_2 detected by time-dependent degenerate four-wave mixing (TD-DFWM) can be manipulated by an additional time-delayed control pulse. By controlling the time delay of this field, we are able to induce varying amounts of additional Rabi cycling among multiple rotational states within the system. The additional Rabi cycling is manifested as a change in the signal detection from homodyne detected to heterodyne detected, depending on the degree of rotational alignment induced. At the highest laser intensities, Rabi cycling among multiple rotational states cannot account for the almost complete transformation to a heterodyne-detected signal, suggesting a second mechanism involving ionization. The analysis we present for these effects, involving the formation of static alignment by Rabi cycling at moderate laser intensities and possibly ion gratings at the highest intensities, appears to be consistent with the experimental findings and may offer viable explanations for the switching from homodyne to heterodyne detection observed in similar DFWM experiments at high laser field intensities ($>10^{13}$ W/cm^2). © *2005 American Institute of Physics*. [DOI: 10.1063/1.1843817]

I. INTRODUCTION

A coherent superposition of eigenstates in an atom or molecule generates a localized wave packet that is nonstationary and evolves in time.[1,2] Realistic energy levels in atoms and molecules lead to a spreading of the wave packet along its trajectory and the loss of localization in space. The wave packet can exhibit revivals and fractional revivals of the initial localization both temporally and spatially.[3] Considerable attention has also been given to forming rotational wave packets and using intense femtosecond lasers to rotationally align molecules by impulsively exciting a superposition of rotational states.[3–7] In this case, the sudden impulse from the short laser pulse transfers angular momentum to the molecule through Rabi cycling, resulting in angular manipulation. The alignment is shown to be maintained even after the laser field is switched off, leading to revivals of the initial alignment at well-defined times. Recently, a number of experiments and theoretical calculations have utilized either sequences of femtosecond laser pulses or tailored femtosecond laser pulses to modify this alignment.[8–13] The present effort focuses on utilizing a time-delayed control pulse to trigger further alignment in O_2 rotational wave packets that are prepared and probed by degenerate four-wave mixing (DFWM).

The wave packet motion is typically tracked along its trajectory using probe techniques that are localized both in space and time, such as absorption, laser-induced fluorescence, and photoionization or photoelectron detection.[14] The use of ion imaging allows one to map out directly the time-dependent angular distribution of a rotational wave packet.[5–7,11,12] Relevant to our work, however, is the use of third-order and higher order nonlinear techniques for probing both gas[15] and liquid[16] phase dynamics, such as DFWM and coherent anti-Stokes Raman scattering. Both techniques utilize the combination of three nonphase-locked laser pulses in a particular phase-matching geometry: the first two fields having initiated some population transfer and/or coherence in the sample, and the third laser pulse probing it through a scattering process.[17,18] These techniques have been successfully applied to study both ground and excited state dynamics of diatomics and polyatomics.[19] Notably in I_2, Schmitt *et al.*[20] demonstrated that FWM can give information about wave packet dynamics on both the ground and excited state potential energy surface while Brown *et al.*[21] showed that selective time delays between the two excitation fields corresponding to multiples of either ground or excited state vibrational periods could lead to optimized population and wave packet transfer between two electronic states.

An intuitive way to explain the origin of a DFWM process is in terms of a transient grating picture where the signal is a result of Bragg scattering of the probe beam by an induced grating of polarized molecules. The first two laser pulses, having wave vectors $\mathbf{k}_1$ and $\mathbf{k}_2$, create an optical interference pattern that imprints a grating onto the medium. The probe beam with wave vector $\mathbf{k}_3$ is then scattered by this polarization grating into the direction satisfying the phase-matching condition, $\mathbf{k}_s=\mathbf{k}_1-\mathbf{k}_2+\mathbf{k}_3$, where $\mathbf{k}_s$ is the wave vector of the scattered field. The grating is transient since the polarized (or aligned) molecules evolve in time, each at a particular angular frequency. The periodic recurrence of initial alignment is manifested by the extent to which the probe beam is Bragg scattered. By monitoring this intensity as a function of time, the dynamics of the excited medium can be inferred.

A few studies using FWM have noted that with increasing pulse intensities the scattering signal transforms from being purely homodyne in nature to a mixture of both homo-

dyne and heterodyne detected.[22,23] The signature for this transformation, as we will see shortly, is typically characterized by an increase in the base line of the FWM signal, with the recurrence profiles dipping below this base line. Of these studies, none have focused on explaining the nature of this effect but have merely incorporated an empirical term in their calculations to account for it.[22,23] In our work, we show how the application of a time-delayed control pulse allows us to manipulate the scattered signal and transform its characteristics from purely homodyne to heterodyne detected. The time dependence of this effect is consistent with the control pulse inducing further Rabi cycling within the ensemble of rotors. We propose how this additional Rabi cycling leads to an enhancement in both the static and dynamic alignment of the molecular system. We suggest how the static alignment can be viewed as a time-independent grating, which Bragg scatters additional probe beam intensity into a similar phase-matching direction as the time-dependent signal. In this way, at the point of its formation, the static grating creates a constant background field source through additional probe scattering (i.e., a local oscillator) which interferes with the time-dependent signal field to heterodyne the observed dynamics. The analysis we present is further corroborated by the recent work of Poulsen *et al.*[24] who suggest that the permanent alignment observed in their experiments on nonadiabatic alignment of asymmetric top molecules using time-resolved photofragment imaging may explain the transformation observed in the FWM signal at increased laser pulse intensities.

To set the scene, we begin by outlining the theory used to model the data presented in the paper. After briefly discussing the experimental setup, we present time-dependent DFWM recurrence data in O_2 as a function of laser intensity (10^{13}–10^{14} W/cm^2). We then show how the application of a time-delayed control pulse affects the FWM signal detected. In particular, we show how the timing of this control pulse is critical in facilitating the transformation from a purely homodyne- to heterodyne-detected signal. Finally we briefly discuss the DFWM dynamics at the highest laser intensities, suggesting another mechanism involving ionization.

II. THEORY

The impulsive excitation of rotational states creates a wave packet that evolves with time. The recurrence time of the polarization depends on the superposed states, arising from Stokes ($\Delta J=+2$) and anti-Stokes ($\Delta J=-2$) nonresonant Raman transitions. The calculations will assume a Boltzmann distribution of rotational states at room temperature, the conditions of the experiments. The time-dependent macroscopic polarization is given by[25]

$$P^{(3)}(t) \propto N\beta^2 \sum_J (p_J - p_{J'}) \frac{(J+1)(J+2)}{(2J+3)} \times \{\sin[2\pi c(\delta\omega_{J,J+2})t]\}\exp(-t/T_2), \quad (1)$$

where J and J' correspond to the initial and final rotational states in the Raman excitation, N is the gas density, and β is the anisotropic polarizability $(\alpha_\parallel - \alpha_\perp)$. $p_J = \exp(-E_J/kT)/Q$ in which E_J corresponds to the energy of the rotational state and Q the rotational partition function. Finally, $\delta\omega_{J,J+2} = \omega_J - \omega_{J+2}$ is the Raman wave number transition (i.e., Stokes transition) while T_2 is the collisional dephasing time. From modeling of the experimental data, we have found that the dependence of the collisional dephasing on rotational state can be neglected. We estimate from the experimental data that the collisional dephasing time is $\approx$75 ps.

The time-dependent DFWM scattering signal $E_s(t)$ is proportional to the third-order macroscopic polarization $P^{(3)}(t)$. The intensity of the FWM signal is directly proportional to the modulus squared of the polarization $|P^{(3)}(t)|^2$ and therefore $|E_s(t)|^2$. The effect of squaring Eq. (1) means that after expanding this expression the signal $|E_s(t)|^2$ will not be composed of the frequency terms of individual Fourier components of the rotational states superposed. Instead, $|E_s(t)|^2$ will be composed of the cross terms arising from the sum and difference frequency terms of the individual Fourier components.[19] As an example, consider four rotational states labeled ω_J, ω_{J+2} and $\omega_{J'}$, $\omega_{J'+2}$. A coherent superposition of each pair of states will generate two rotational Raman wave packets with beat frequencies A and B (where $A=\omega_J-\omega_{J+2}$ and $B=\omega_{J'}-\omega_{J'+2}$). Unlike in a pump/probe experiment where one detects the individual beat frequencies A and B, the frequencies detected here correspond to $A\pm B$, $2A$, and $2B$. This leads to two progressions in the fast Fourier transform of the rotational recurrence scans [see Fig. 2(d)], the first being $A-B$ and the second $A+B$, $2A$, and $2B$. The accidental degeneracies arising from cross terms of all the rotational state superpositions in the ensemble lead to a more intense $A-B$ progression. Detection of only the scattered signal in this way is termed homodyne detection.

In order to observe more strongly a signal that depends on the individual frequency terms A and B (the individual Fourier components of the rotational states superposed), one can coherently mix, or heterodyne detect the signal field by combining it with a reference field of similar wavelength, termed a local oscillator $E_{\mathrm{LO}}(t)$. The local oscillator can be part of the probe beam, or some other field, and appears as a constant background source. The signal is now proportional to $|E_s(t)+E_{\mathrm{LO}}(t)|^2$. If we expand this expression, we see that in addition to the beat frequencies arising from the $|E_s(t)|^2$ term, we also have terms arising from $|E_s(t)E_{\mathrm{LO}}(t)|$ and $|E_{\mathrm{LO}}(t)|^2$. The former corresponds to measurement of the individual quantum beats (A and B), essentially $|E_s(t)|$, while the latter is a constant. Consequently, as the local oscillator increases in magnitude, the signal changes from being homodyne to heterodyne detected. A modified form of Eq. (1) incorporating an empirical variable k to account for the heterodyne detection, which is dependent on the magnitude of the local oscillator $E_{\mathrm{LO}}(t)$ can be expressed as[25]

$$|P'^{(3)}(t)|^2 \propto \left| N\beta^2 \sum_J (p_J - p_{J'}) \frac{(J+1)(J+2)}{(2J+3)} \times \{\sin[2\pi c(\delta\omega_{J,J+2})t]\}\exp(-t/T_2) + k \right|^2. \quad (2)$$

It is important to note that the homodyne component of the signal will always be present but the relative magnitudes between the homodyne and heterodyne components of the

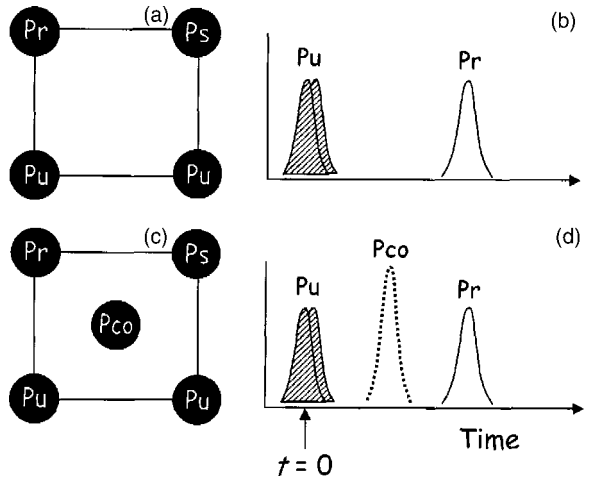

FIG. 1. (a) A schematic diagram illustrating the pulse arrangement of the pump (Pu) and probe (Pr) beams in the forward boxcar configuration. (b) depicts the temporal arrangement of these beams. The two pump beams are overlapped temporally to form a transient grating. This defines time zero for all experiments. The probe pulse is scanned in incremental steps (typically 0.05 ps) up to a maximum delay of 100 ps. (c) and (d) are similar to (a) and (b) but with the inclusion of the control pulse (Pco). (c) The control pulse occupies the center of the box while (d) illustrates the relative timings of all four pulses.

signal will change depending on the value of the local oscillator. A goal of this paper is to present evidence for the physical origin of the empirical factor *k*.

At the moderately high laser field intensities where the experiments have been carried out (10^{13}–10^{14} W/cm^2), multiple Rabi cycling occurs whereby an initially populated rotational state can undergo a series of two-photon transitions accessing higher (or lower) rotational states. As we will see in Sec. IV, such a process can lead to the formation of static or permanent alignment, which can Bragg scatter probe light into the same phase-matching direction as the transient grating. As this is a constant field source, it can, in principle, behave as a local oscillator. Equations (1) and (2) do not include any effects of laser intensity and therefore we seek an alternative approach to account for this to compare to experiments. It has been shown by Ortigoso *et al.*[26] that the final amplitudes of each rotational state, after the interaction with an intense laser field pulse, can be accurately evaluated by solving the following Hamiltonian of a molecule subject to an intense laser field,

$$H_{\mathrm{eff}}(t) = B\mathbf{J}^2 - \tfrac{1}{2}\varepsilon^2(t)[(\alpha_{\parallel} - \alpha_{\perp})\cos^2\theta + \alpha_{\perp}], \tag{3}$$

where $\mathbf{J}^2$ is the squared angular momentum operator, B the rotational constant, and $\varepsilon(t)$ the time-dependent laser electric field, assumed Gaussian. θ is the polar angle between the molecular axes and the electric field, while $\alpha_{\parallel}$ and $\alpha_{\perp}$ are the components of the static polarizability parallel and perpendicular to the molecular axes.

Using the same formalism as detailed by Ortigoso *et al.*,[26] the evolution of the molecular wave function during the aligning pulse is evaluated by numerically integrating a set of coupled differential equations connecting rotational states differing by $\Delta J = 0, \pm 2$ using the Runge–Kutta method.[26] The aligning pulse is assumed to have a Gaussian pulse shape of the form, $g(t) = \exp(-t^2/\sigma^2)$, characterized by a full width at half maximum, $\tau \cong (5/3)\sigma$, where τ corresponds to the pulse duration. The common measurement of alignment, $\langle\Psi(t)|\cos^2\theta|\Psi(t)\rangle$, can then be computed with the evaluated amplitude coefficients of each rotational state to give

$$\begin{aligned}\langle\cos^2\theta\rangle &= \langle\Psi(t)|\cos^2\theta|\Psi(t)\rangle \\ &= \sum_{J,M} |a_J|^2 C_{J,J,M} + |a_J| \\ &\quad \times |a_{J+2}|\cos(\delta\omega_{J,J+2,M}t) C_{J,J+2,M},\end{aligned} \tag{4}$$

where $|a_J|$ and $|a_{J+2}|$ are the contributing amplitudes of the individual rotational states in the superposition after the laser pulse-molecule interaction and

$$\begin{aligned}C_{J,J,M} &= \langle J,M|\cos^2\theta|J,M\rangle, \\ C_{J,J+2,M} &= \langle J,M|\cos^2\theta|J+2,M\rangle,\end{aligned} \tag{5}$$

in which $\delta\omega_{J,J+2}$ are the Stokes Raman wave number transitions. The calculations described assumed an initial Boltzmann distribution of rotational states at room temperature. To obtain numerical convergence, 39 rotational states were typically included in these calculations for comparison to experiments.

III. EXPERIMENT

The laser is a commercial Spectra-Physics system consisting of a Ti-sapphire oscillator and a regenerative amplifier. The system delivers 0.8 mJ pulses centered at 805 nm at 1 kHz repetition rate. The measured pulse duration is 50 fs. The laser output is split into four beams: two pump beams (Pu), one probe beam (Pr), and one control beam (Pco). The intensity of the pump, probe, and control beams could be individually varied using neutral density filters with negligible effects on the spectral and temporal profiles, verified with a spectrometer (Ocean Optics HR2000) and single-shot autocorrelator, respectively. The pump and probe beams were kept equal in energy and varied from 35 μJ per pulse up to 120 μJ per pulse, while the control beam was maintained at 300 μJ per pulse. The pump and probe beams were combined at the sample in the forward boxcar geometry by a 400 mm focal length lens. At the lens, these three beams occupy three corners of a square with $\approx$2 cm sides. The control beam occupies the center of the square. The beam diameters at the interaction region are 110–120 μm. With this setup, there are two-pulse arrangements, one without the control pulse and one with the control pulse. The two-pulse arrangements and their timings are illustrated in Figs. 1(a)–1(d), respectively. The relative delay between the pump pair is kept fixed and overlapped in time, while the delays of both the probe and control beams are changed using motor controlled delay stages (Physik-Instrumente). The probe is typically varied over 100 ps with a minimum step size of 0.05 ps while the control beam is fixed at particular delays relative to the pump beams (up to 7 ps delay). Both stages had a design resolution better than 0.1 μm (0.3 fs).

The sample of O_2 (1 atm pressure) is contained in a gas cell 50 cm in length. The temporal and spatial overlap of all four beams is found by focusing all four attenuated beams

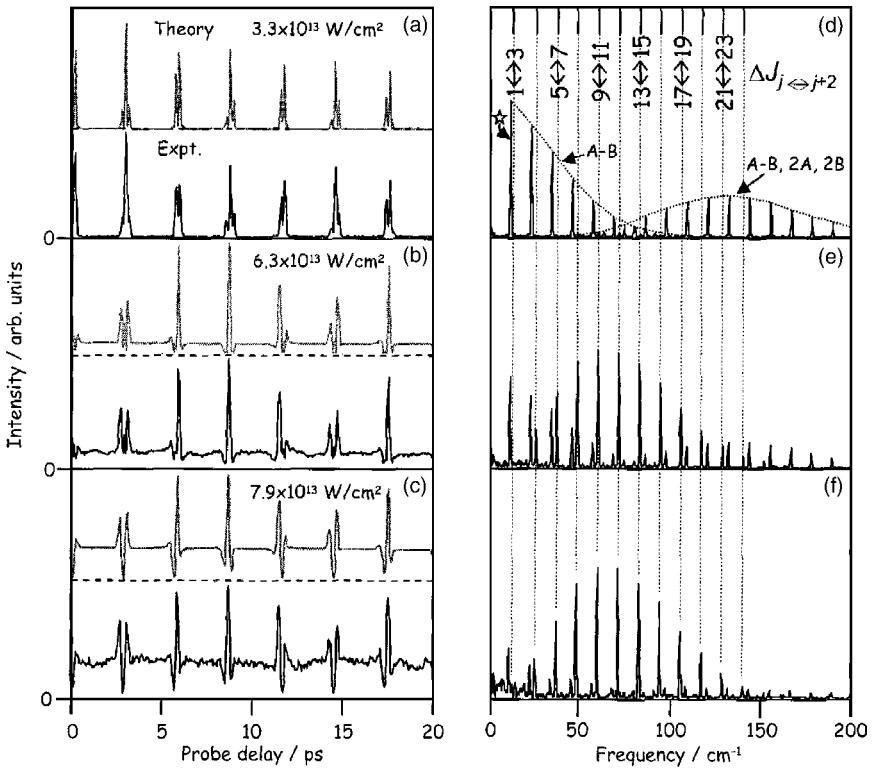

FIG. 2. Time-resolved rotational recurrence data [(a), (b), and (c)] and the corresponding FFTs [(d), (e), and (f)] for three different laser intensities, 3.3×10^{13}, 6.3×10^{13}, and 7.9×10^{13} W/cm^2 respectively. (a), (b), and (c), each show two plots that correspond to experiment (bottom) and theory (top). The theoretical plots are modeled using Eq. (2) with their base line indicated by a dashed horizontal line. These plots were obtained using 0, 0.35, and 1 for the values of k for (a), (b) and (c), respectively. (d), (e), and (f) are the FFTs of the experimental recurrence plots. Two progressions are observed in (d) indicated by the dotted lines. The two progressions arise from squaring Eq. (1) and are labeled $A-B$ and $A+B$, $2A$, $2B$, respectively (see text for details). The star in (d) denotes the rotational recurrence time appearing at 11.44 cm^{-1}. The dashed vertical lines are the wave number values of the beat frequencies between the pairs of rotational states the wave packet is composed of (A or B). (f) shows essentially a single series that matches perfectly with these beat frequencies (labeled A and B in the text). The transformation from a homodyne-detected to a heterodyne-detected signal [from (d) to (f)] is the main focus of the paper.

into a 0.2 mm thick BBO crystal. When overlapped, a matrix of equally spaced UV beams is seen after the crystal, a result of second and higher order wave mixing occurring in the crystal at the appropriate phase-matching direction. The crystal is then replaced by the gas cell. After passing through another 400 mm lens, the pump, probe, and control beams are blocked by a mask while the FWM scattered signal (labeled Ps in Fig. 1) is collected onto a photodiode and directed to a fast oscilloscope (LeCroy waverunner LT372) without any spectral filtering. Data acquisition is achieved through a general purpose interface bus (GPIB) connected to a computer running LABVIEW.

IV. RESULTS AND DISCUSSION

Figure 2 shows experimental plots (bottom plots) of rotational recurrences in O_2 for three different pump (Pu) laser pulse intensities, 3.3×10^{13}, 6.3×10^{13}, and 7.9×10^{13} W/cm^2 [Figs. 2(a)–2(c), respectively]. In all three sets of recurrence data, one clearly sees periodic peaks spaced by $\approx$2.9 ps. The time delay between rotational recurrences occurs with a periodicity of $1/2B_0c$, where B_0 is the rotational constant [1.438 cm^{-1} (Ref. 27)] and c the speed of light, which corresponds to the phase factors of all the component wave functions that make up the wave packet advancing by the same amount in modulo 2π. Rotational recurrences may also occur at fractions of the recurrence time, the details of which are clearly described by Dooley *et al.*[28] For molecules where both odd and even J states are equally populated, recurrences occur spaced by $1/4B_0c$, however, when only odd or even states are populated, the spacing between recurrences becomes $1/8B_0c$. The periodicity however still remains as $1/2B_0c$. Since O_2 has a nuclear spin of 0, the total wave function must be symmetric to nuclear exchange. As a result, rotational states with even J are missing and the usual period of $1/2B_0c$ becomes $1/8B_0c$, in excellent agreement with our data. It is clearly evident from the figures how the profiles of the recurrences change as a function of laser intensity, as manifested by an elevated base line and the recurrences dipping below the base line at the highest laser intensity. This is understood to be a change in the relative ratio of the signal strengths for the $1/8B_0c$ ensemble average recurrences (labeled $A-B$ and $A+B$, $2A$, $2B$ above) versus the signal strength of the individual pairs of quantum beats between rotational states (labeled A or B).[22,23] The former occurs in the homodyne detection while the latter is accentuated in the heterodyne detection. The corresponding theoretical plots (top plots) for the recurrences modeled using Eq. (2) are also shown with the base line indicated by a dashed line. By including the effects of a variable-strength local oscillator through the constant k, the experimental data is fit very well. One can estimate the relative magnitude of the scattered probe field to the local oscillator and find that, at 7.9

$\times 10^{13}$ W/cm^2 for instance, the relative magnitudes of the scattered field and local oscillator are comparable.

The changes in the O_2 coherent spectral features underlying the recurrence data are seen more clearly in the fast Fourier transforms (FFT) of the recurrence data. Figures 2(d)–2(f) correspond to the recurrence data of Figs. 2(a)–2(c), respectively. They show how the increasing electric field of the pump/probe beams leads to the enhancement of the signal intensities of the individual beat frequencies (A and B previously) of various pairs of rotational states composing the wave packet (dashed vertical lines). At 3.3 $\times 10^{13}$ W/cm^2, the FFT shows two progressions of equidistant lines. For a detailed explanation regarding the origin of these progressions, the reader is referred to the article by Frey *et al.*[29] Briefly, the two sequences arise from squaring Eq. (1). The first sequence is attributed to the difference frequencies of the states superposed while the second sequence, shifted to higher energies, is due to both the sum frequencies and twice the individual frequencies of the superposed states [labeled $A-B$ and $A+B$, $2A$, $2B$, respectively in Fig. 2(d)]. The rotational recurrence time $1/8B_0c$ appears in the FFT at 11.44 cm^{-1} and is indicated by a star on Fig. 2(d). At 6.3 $\times 10^{13}$ W/cm^2, another sequence begins to appear. This sequence coincides with the beat frequencies of the individual pairs of states in the superposition (labeled A or B above) and dominates at the highest laser intensity. The fact that these beat frequencies emerge corresponds to the fact that the local oscillator E_{LO} increases in magnitude and transforms the signal to heterodyne detected.

The remainder of the paper tries to understand the mechanism governing the appearance of the local oscillator in the O_2 experiments. The questions we will answer include whether the local oscillator is a result of some molecular property or some additional scattering process, whether we are able to manipulate the transformation from homodyne to heterodyne detection using a control pulse, and what are the underlying physics behind the effects of the control pulse? We will show how the timing of the control pulse is critical to trigger a transformation from homodyne to heterodyne detection, providing very strong evidence as to the origin of the local oscillator.

First, we can eliminate the effect of optical scattering of the two pump beams from the entrance and exit faces of our sample cell since the measured transient grating response of fused silica is instantaneous in time[30] and can only occur near time zero. Similarly, optical heterodyning from scatter of the probe can also be eliminated. A set of experiments were carried out in which the probe beam intensity was varied while keeping the intensity of the pump beams fixed (3.3×10^{13} W/cm^2). The recurrence spectra recorded showed no indication of optical heterodyning. This suggests that the heterodyning is caused by the pump beams in the gas sample and does not involve additional scattering processes.

Seideman[3] and Stapelfeldt and Seideman[31] have shown that, with increasing laser intensities, Rabi cycling between J states can occur where various excitations (to higher J) and deexcitations (to lower J) lead to significant changes in J state distributions relative to a thermal Boltzmann distribution. Raman deexcitations have a lower limit of $J=1$ for O_2,

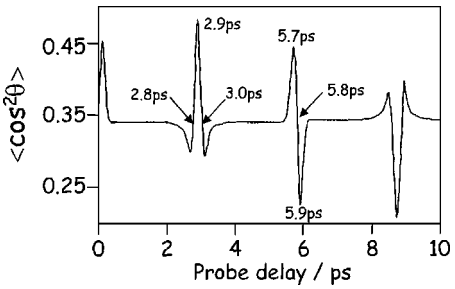

FIG. 3. Theoretical plot of the alignment parameter $\langle\cos^2\theta\rangle$ as a function of time for O_2. The plot is calculated using Eq. (4) and assuming a laser field intensity of 2.7×10^{13} W/cm^2. Alignment corresponds to values of $\langle\cos^2\theta\rangle > 1/3$ while antialignment corresponds to values of $\langle\cos^2\theta\rangle < 1/3$. Also indicated on this plot are the delay times where the control pulse (Pco) is sent in for the data presented in Figs. 4 and 5.

while for Raman excitations, no restriction applies. From here on, we call this rotational ladder climbing. As a result, the average J of the rotational ensemble can be significantly greater than the thermal average J before the laser/molecule interaction, i.e., $J_{\mathrm{ensemble}} > J_{\mathrm{thermal}}$. The M state distribution, however, should transfer over from lower J to higher J ($\Delta M=0$ for linearly polarized light). Because of this, there is no longer a uniform distribution of M values, leading to additional alignment that is permanent, i.e., stationary, which has been experimentally verified by a number of research groups.[6,7,24]

We first hypothesize that the permanent alignment associated with Rabi cycling in O_2 can serve as a molecular local oscillator. Then we perform experiments to corroborate this hypothesis. In these experiments, permanent alignment can be viewed as a static grating. As with the transient grating that scatters probe light in a time-dependent fashion, the static grating can scatter probe radiation into the same phase-matching direction as the time-dependent signal, but the scattering intensity is independent of time. The constant scatter from the static grating is coherent and can interfere with the time-dependent scatter of the probe. In this way, permanent alignment serves as a local oscillator.

To see if rotational ladder climbing in O_2 is actively heterodyning our signal, we carried out a series of two-pulse alignment experiments by first exciting a rotational wave packet under weak-field conditions, 2.7×10^{13} W/cm^2 (i.e., no optical heterodyning), with the pump grating pair and then applying a second control pulse (5.7×10^{13} W/cm^2), at well-defined time delays. Experiment[11,12] and theory[13] have shown that the control pulse initiates additional Rabi cycling leading to an increase in either alignment or antialignment (molecular axis aligned either parallel or perpendicular to laser field) depending on the time delay and is more pronounced around rotational recurrences. Therefore, by monitoring the extent of optical heterodyning, if any, as a function of control pulse delay, we intend to determine whether additional Rabi cycling is the operative mechanism here.

A theoretical plot of the alignment parameter $\langle\cos^2\theta\rangle$ as a function of time is shown in Fig. 3 for O_2. The plot is calculated from Eq. (4), assuming a laser field intensity of 2.7×10^{13} W/cm^2. The role of Fig. 3 is twofold: First, it illustrates the timing of the control pulse relative to the pump

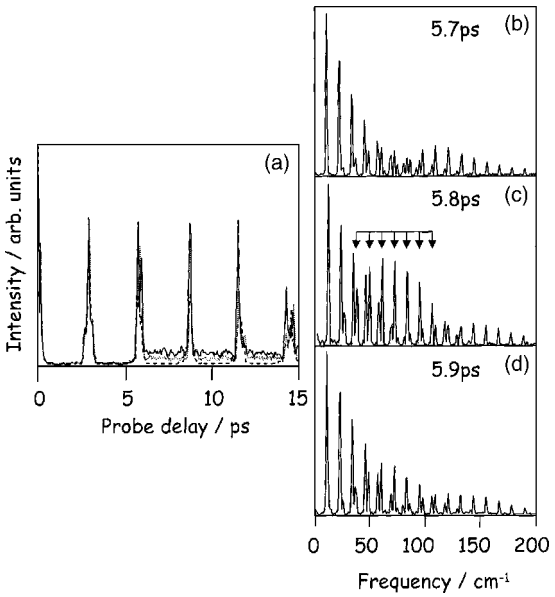

FIG. 4. (a) Rotational recurrence plots for three different delays of the control pulse, 5.7, 5.8, and 5.9 ps (long dashes, solid line, and short dashes, respectively). The pump/probe and control pulses were kept at 2.7×10^{13} and 5.7×10^{13} W/cm^2, respectively. (b), (c), and (d) correspond to FFTs of recurrence signals at these delays. Notice in (c) the emergence of an additional sequence of peaks, indicated by a comb of arrows. This points towards a switching from homodyne to heterodyne detection. The step in the base line (a) is indicative of additional scatter of the probe which is hypothesized as being caused by an additional, time-independent grating. This results from permanent alignment of the O_2 molecules through enhanced Rabi cycling after the interaction with the intense control field. This can serve as a local oscillator to heterodyne the signal.

grating pair. Second, it serves to aid the discussions that will follow from the data presented in Figs. 4 and 5. Figure 4(a) shows three recurrence plots where the control pulse was sent in at 5.7, 5.8, and 5.9 ps delays, as indicated in Fig. 3. The most striking feature of this plot is the sudden increase in the base line when the control pulse is sent in at 5.8 ps delay. The sudden increase in the base line is indicative of additional probe scatter into the correct phase-matching direction along the detector. We have verified that the additional scatter occurs only when all four beams are present and vanishes when each of the pump, control, and probe beams is blocked individually. In addition to the rotational recurrence spectra, the FFTs at these delays are also shown in Figs. 4(b)–4(d). It is clearly evident that when the control pulse is sent in at 5.8 ps after the grating pair, an additional sequence of lines appears (as indicated by the comb of arrows) coinciding with the beat frequencies of individual pairs of rotational states in the wave packet superposition (those labeled *A* or *B* previously). It is interesting to note the similarities between Fig. 4(c) with Fig. 2(e).

The fact that enhanced Rabi cycling occurs when an intense control pulse is incident on an already-aligned sample provides strong support for the appearance of the base line shift in O_2. By rotational ladder climbing, we increase both the time-dependent and the time-independent alignment. Although the FWM detection does not allow us to measure the extent of alignment quantitatively, as is possible by photofragment imaging, we can rule out most of the possible causes of a base line shift, such as additional scatter from the control pulse or congestion in the time domain due to additional pairs of rotational beats excited (by simulation of the signal). This leaves us with the most probable cause, that is, an increase in the formation of a static grating through permanent alignment, enabling additional scatter of the probe. In fact, the most effective time delay for the control pulse to enhance Rabi cycling is at the point of a recurrence when the molecules are neither aligned nor antialigned, i.e., when $\langle\cos^2\theta\rangle=1/3$. This is because the molecules that are moving towards alignment/antialignment experience, in classical terms, a greater impulsive force or torque from the control pulse leading to an increase in their average rotational energy. This effect has been observed recently by Lee *et al.*[11] While there is a clear enhancement in their dynamic alignment/antialignment,[11] there is no indication in their results that there is an increase in the permanent alignment. Our detection setup, employing the forward boxcar technique, is a background free technique and hence is very sensitive to measuring any additional scatter that may be caused by the formation of a static grating. The number density of molecules is also orders of magnitude greater than those of molecular beams. It is therefore likely to be these experimental differences that allow us to detect the signature of an enhancement in the permanent alignment of the molecules. We also performed an FFT of time slices of the O_2 recurrence data to see if the heterodyne component shows any time dependence. As far as we can tell, there are no apparent changes in the extent to which the data are heterodyned versus time. This suggests that it is very unlikely that a dynamic alignment is somehow causing this transformation from homodyne to heterodyne detected.

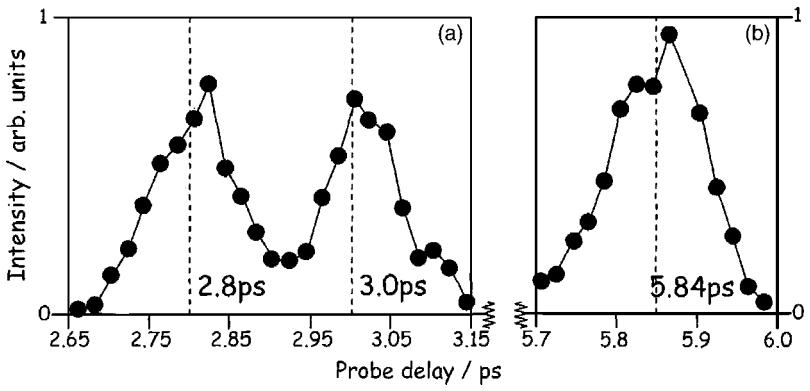

FIG. 5. Variation in the base line intensity as the control pulse is scanned through two successive recurrences (2.9 and 5.8 ps). (a) corresponds to the probe pulse fixed at 4 ps while the control pulse is scanned from 2.65 to 3.15 ps while (b) corresponds to the probe pulse fixed at 7 ps and the control pulse scanned from 5.7 through 6.0 ps. Note that no spectral averaging is employed and the lines through the points serve to guide the eye. The base line is seen to rise to a maximum around the recurrence time.

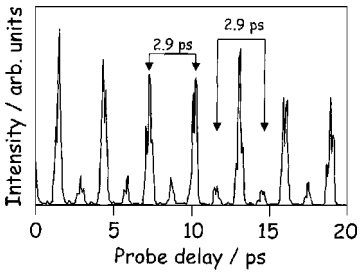

FIG. 6. Rotational recurrence plot in which the control pulse is sent into the sample 1.45 ps prior to the grating pair pulses. Peaks appear at twice the recurrence period (see text for details). The alternating intensities (≈4:1) result from the twofold difference in intensity of the control and grating pulses, respectively.

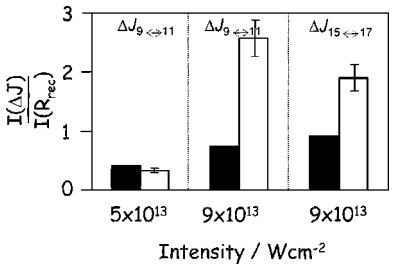

FIG. 7. Histogram plot depicting the change in the peak ratios of the calculated (solid blocks) and measured (open blocks) FFTs for the most intense rotational state superposition peak ΔJ and the rotational recurrence peak (R_{rec} at 11.44 cm^{-1}). The data are for two field strengths of the pump pulses corresponding to 5×10^{13} and 9×10^{13} $\mathrm{W/cm}^2$.

To confirm the enhancement in the base line, a series of experiments were conducted in O_2 in which the probe pulse was first fixed at 7 ps (Fig. 5). At this time, there are no rotational recurrence peaks present. The delay of the control pulse was then scanned between 5.7 and 6.0 ps to map out the shift in the base line signal as a function of time delay. Figure 5(b) shows that the peak in the base line shift is indeed around 5.84 ps, which is nearly in perfect agreement with the predicted value of 5.82 ps (crossover between alignment and antialignment). The small discrepancy (20 fs) is well within the resolution of our laser pulse duration (50 fs). We have also carried out similar experiments at different time delays. Figure 5(a) corresponds to a fixed probe delay of 4 ps (again, not a rotational recurrence peak) while the control pulse is scanned between 2.65 and 3.15 ps. Two peaks are apparent, corresponding to the symmetric peak in the $\langle\cos^2\theta\rangle$ function (Fig. 3). Once again, the peaks appear at the two crossover points between alignment and antialignment; since there are two crossover points with similar slopes, we observe two equally intense peaks in our signal. The magnitudes of the peak heights in the two spectra [Figs. 5(a) and 5(b)] are slightly different. The peak in Fig. 5(b) is greater than either of the two peaks in Fig. 5(a). At the crossing point, the molecules are essentially all in phase at 5.8 ps, while at 2.8 and 3.0 ps they are either nearly in phase or beginning to move out of phase. The effectiveness of the control pulse at further aligning the molecules is less pronounced therefore, which is manifested in the peak intensities.

It is worth noting that Comstock, Senekerimyan, and Dantus[22] proposed that heterodyning of their time-resolved transient grating data in CO_2 at high laser fields is likely caused by plasma formation, which emits a continuous, spectrally shifted light pulse that decays on a very long time scale (1 ns). The light pulse, emitted also in the phase-matching direction in which the FWM signal is formed, can interfere with the FWM signal and heterodyne it. It seems unlikely that this is the mechanism operating here. We tested this by sending the control pulse into the O_2 sample prior to the grating pair to initiate a plasma emission. Figure 6 shows a rotational recurrence signal in which the control pulse is sent in 1.45 ps prior to the grating pair. Recurrences are now observed at twice the frequency of the single pulse experiments, with alternating intensities, but minimal optical heterodyning is observed in the FFT (not shown). If the plasma emission had served as a local oscillator, the signal would show optical heterodyning. Interestingly, the control pulse creates a spatially uniform distribution of alignment in the sample in this case and not a grating of alignment. After 1.45 ps delay, the ensemble of rotors become isotropically distributed (half the rotational recurrence time). At this time, the grating pair (Pu), now incident on the sample, imposes a grating of alignment. However, in the spatial areas of destructive interference caused by the optical interference of the pump beams, the aligned molecules created by the control pulse are unaffected, i.e., their coherence is preserved. As a result, two gratings are essentially present in the sample resulting in two series, time shifted by half the rotational recurrence period. The alternating intensities are a result of the control pulse being twice as intense as the grating pair. Since these are two-photon Raman excitations, the signal is observed to increase approximately fourfold.

Thus, permanent alignment seems a plausible mechanism to explain the optical heterodyning of the signal in the O_2 experiments. The effects of higher intensity control fields were studied to determine whether the signal can be completely switched from homodyne to heterodyne detected, as is evident in Fig. 2(f). We found however that, beyond control pulse intensities of 5.7×10^{13} $\mathrm{W/cm}^2$, the transient grating signal significantly diminishes, most probably caused by the detrimental effects from the high peak power of the control pulse, such as plasma formation. This still leaves us with the question of whether or not the almost complete transformation to heterodyne-detected signal observed in Fig. 2(f) can be attributed solely to permanent alignment. In order to explore this further, we calculated how the alignment parameter $\langle\cos^2\theta\rangle$ varies as a function of laser field intensity using Eq. (4). This allows us to assess the extent of Rabi cycling through multiple Raman excitations. These calculations did not include the effects of a control pulse, and we also assumed the homodyne-detected signal to be directly related to the square of the alignment parameter $\langle\cos^2\theta\rangle$, since for heterodyne detection the signal is proportional to $\langle\cos^2\theta\rangle$.[32]

The histogram in Fig. 7 summarizes the main results of these calculations. The solid blocks represent calculations obtained by evaluating Eq. (4) while the open blocks represent experimental data. The intensity of each block corresponds to the ratio between the most intense individual beat

frequency observed in the experiment (e.g., superpositions between $\Delta J_{9\leftrightarrow 11}$) and the rotational recurrence peak (at $11.44\ \mathrm{cm}^{-1}$) from the FFTs. At a low intensity ($5\times 10^{13}\ \mathrm{W/cm}^2$), the experiment is modeled almost perfectly by the theory. However, at the higher intensity ($9\times 10^{13}\ \mathrm{W/cm}^2$), a significant enhancement in the individual beat frequency peak relative to the rotational recurrence peak is observed experimentally, which the theory cannot reproduce. Interestingly, the calculation gives as its most intense peak $\Delta J_{15\leftrightarrow 17}$. This is not surprising since further Rabi cycling at increasing laser fields can access higher and higher rotational state superpositions. The experiment however shows no such obvious trend. What this implies is that at higher laser fields, permanent alignment through Rabi cycling cannot solely account for the almost complete heterodyne-detected signal in O_2 that is evident in Fig. 2(f) and suggests that another mechanism is operative at higher field strengths.

We have carried out measurements of ion signal production in O_2 as a function of laser intensity and have observed that the production of O_2 ions emerges at intensities in excess of $7\times 10^{13}\ \mathrm{W/cm}^2$, coinciding with the almost complete heterodyning of the data [Figs. 2(c) and 2(f)]. Thresholds in O_2 ion production, similar to the ones here, have been observed in previous experiments.[33] Although at this point this is merely conjecture, at these intensities the formation of a stationary ion grating could begin to occur that has the same spatial interference pattern as the transient grating. Since the optical properties of the medium are different for ions and neutrals (namely, the refractive index), the ion grating could also cause Bragg scattering of additional probe into the same phase-matching direction as that of the transient grating of aligned molecules. The additional scattered field, once again coherent, would interfere with the time-dependent scatter to heterodyne it. The ion grating mimics the thermal gratings that have been observed by previous research groups.[34,35] In particular, Vöhringer and Scherer[30] showed how thermal gratings could be a source of further diffraction in the correct scattering geometry analogous to the ion grating mechanism we suggest here.

It is important to note here that a stationary ion grating could not be invoked to explain the changes observed in the signal at lower field strengths. The control pulse experiments conclusively show that the switching from homodyne to heterodyne detection at lower intensities occurs at times when the molecules are approaching alignment or antialignment. If an ion grating were operative, the switching would occur at the point when the molecules were aligned with the electric field of the control pulse, since this corresponds to the maximum in the ionization cross section and hence the maximum ion production.[7]

V. SUMMARY AND CONCLUSION

DFWM signals in O_2 show a marked dependence on laser intensity. As the laser intensity increases, the FWM signal clearly switches from homodyne to heterodyne detected. The switching implicates the presence of a local oscillator that interferes with the scattered probe beam and heterodynes it. The local oscillator, at moderate laser intensities, is very likely to arise from the molecular properties of the system and is not a result of some additional background scattering or plasma formation.

By employing a fourth, more intense laser field as a control pulse, we can effectively trigger the creation of the local oscillator and switch the signal detection from homodyne to heterodyne detected. The experimental findings are consistent with the idea that the control pulse enhances the molecular alignment of the ensemble by inducing further Rabi cycling and alignment among the rotors. The increased rotational energy results in the formation of a static grating of permanent alignment, which serves to scatter additional probe light into the correct phase-matching direction to heterodyne the signal. The consistency of this model is evident from the time dependence of the control pulse process. The effectiveness of the control pulse is, by far, more pronounced around times corresponding to the recurrence of the rotational wave packet. In particular, when the revived wave packet is approaching alignment or antialignment ($\langle\cos^2\theta\rangle = 1/3$), the homodyne to heterodyne transformation is clearly evident.

At high laser intensities ($>7\times 10^{13}\ \mathrm{W/cm}^2$), permanent alignment through Rabi cycling cannot solely account for the almost complete conversion to a heterodyne-detected signal [Figs. 2(c) and 2(f)]. The observed heterodyning of the signal must be accounted for in some other way. At these intensities, the threshold for ionization is already reached leading to a catastrophic modification of the sample. The ions that are formed within the grating serve as an additional scattering source. This is further corroborated by work carried out in H_2, which will be the topic of a future publication.[36]

ACKNOWLEDGMENTS

The authors thank Professor Marcus Dantus and Matthew Comstock for providing them with Ref. 22 prior to its publication and for advice about the ionization mechanism. Experimental assistance from Dr. Stefan Gilb and Alan Arrowsmith is also greatly appreciated. This work was supported by the Director, Office of Science, Office of Basic Energy Sciences, Chemical Sciences, Geosciences and Biosciences Division, U.S. Department of Energy under Contract No. DE-AC03-76SF00098.

[1] I. S. Averbukh and N. F. Perelman, Phys. Lett. A **139**, 449 (1989).
[2] J. Wals, H. H. Fielding, and H. B. van Linden van den Heuvell, Phys. Scr., T **T58**, 62 (1995).
[3] T. Seideman, Phys. Rev. Lett. **83**, 4971 (1999).
[4] W. Kim and P. M. Felker, J. Chem. Phys. **104**, 1147 (1996).
[5] J. J. Larsen, I. Wendt-Larsen, and H. Stapelfeldt, Phys. Rev. Lett. **83**, 1123 (1999).
[6] F. Rosca-Pruna and M. J. J. Vrakking, Phys. Rev. Lett. **87**, 153902 (2001).
[7] I. V. Litvinyuk, K. F. Lee, P. W. Dooley, D. M. Rayner, D. M. Villeneuve, and P. B. Corkum, Phys. Rev. Lett. **90**, 233003 (2003).
[8] J. G. Underwood, M. Spanner, M. Yu. Ivanov, J. Mottershead, B. J. Sussman, and A. Stolow, Phys. Rev. Lett. **90**, 223001 (2003).
[9] M. Spanner, E. A. Shapiro, and M. Ivanov, Phys. Rev. Lett. **92**, 093001 (2004).
[10] M. Renard, E. Hertz, B. Lavorel, and O. Faucher, Phys. Rev. A **69**, 043401 (2004).
[11] K. F. Lee, I. V. Litvinyuk, P. W. Dooley, M. Spanner, D. M. Villeneuve, and P. B. Corkum, J. Phys. B **37**, L43 (2004).

[12]C. Z. Bisgaard, M. D. Poulsen, E. Péronne, S. S. Viftrup, and H. Stapelfeldt, Phys. Rev. Lett. **92**, 173004 (2004).
[13]M. Leibscher, I. Sh. Averbukh, and H. Rabitz, Phys. Rev. Lett. **90**, 213001 (2003).
[14]A. H. Zewail, in *Femtochemistry*, edited by A. H. Zewail (World Scientific, Singapore, 1994), Vols. I and II.
[15]V. V. Lozovoy, I. Pastirk, E. J. Brown, B. I. Grimberg, and M. Dantus, Int. Rev. Phys. Chem. **19**, 531 (2000).
[16]M. D. Fayer, Annu. Rev. Phys. Chem. **33**, 63 (1982).
[17]S. Mukamel, *Principles of Nonlinear Optical Spectroscopy* (Oxford University Press, New York, 1995).
[18]Y. R. Shen, *The Principle of Nonlinear Optics* (Wiley, New York, 1984).
[19]E. J. Brown, Q. Zhang, and M. Dantus, J. Chem. Phys. **110**, 5772 (1999).
[20]M. Schmitt, G. Knopp, A. Materny, and W. Kiefer, Chem. Phys. Lett. **270**, 9 (1997).
[21]E. J. Brown, I. Pastirk, B. I. Grimberg, V. V. Lozovoy, and M. Dantus, J. Chem. Phys. **111**, 3779 (1999).
[22]M. Comstock, V. Senekerimyan, and M. Dantus, J. Phys. Chem. A **107**, 8271 (2003).
[23]V. V. Matylitsky, W. Jarzęba, C. Riehn, and B. Brutschy, J. Raman Spectrosc. **33**, 877 (2002).
[24]M. D. Poulsen, E. Péronne, H. Stapelfeldt, C. Z. Bisgaard, S. S. Viftrup, E. Hamilton, and T. Seideman, J. Chem. Phys. **121**, 783 (2004).
[25]B. Lavorel, O. Faucher, M. Morgen, and R. Chaux, J. Raman Spectrosc. **31**, 77 (2000).
[26]J. Ortigoso, M. RodrÍguez, M. Gupta, and B. Friedrich, J. Chem. Phys. **110**, 3870 (1999).
[27]H. M. Frey, P. Beaud, T. Gerber, B. Mischler, P. P. Radi, and A. P. Tzannis, J. Raman Spectrosc. **31**, 71 (2000).
[28]P. W. Dooley, I. V. Litvinyuk, K. F. Lee, D. M. Rayner, M. Spanner, D. M. Villeneuve, and P. B. Corkum, Phys. Rev. A **68**, 023406 (2003).
[29]H. M. Frey, P. Beaud, T. Gerber, B. Mischler, P. P. Radi, and A. P. Tzannis, Appl. Phys. B: Lasers Opt. **68**, 735 (1999).
[30]P. Vöhringer and N. F. Scherer, J. Phys. Chem. **99**, 2684 (1995).
[31]H. Stapelfeldt and T. Seideman, Rev. Mod. Phys. **75**, 543 (2003).
[32]V. Renard, M. Renard, S. Guérin, Y. T. Pashayan, B. Lavorel, O. Faucher, and H. R. Jauslin, Phys. Rev. Lett. **90**, 153601 (2003).
[33]D. Normand, C. Cornaggia, J. Lavancier, J. Morellec, and H. X. Liu, Phys. Rev. A **44**, 475 (1991).
[34]C. C. Hayden and R. Trebino, Appl. Phys. B: Photophys. Laser Chem. **51**, 350 (1990).
[35]P. A. Delve and B. J. Whitaker, Phys. Chem. Chem. Phys. **2**, 5594 (2000).
[36]V. G. Stavros, E. Harel, and S. R. Leone (unpublished).